31st Annual International Conference of the IEEE EMBS
Minneapolis, Minnesota, USA, September 2-6, 2009

Metal Artifact Suppression from Reformatted Projections in Multi-slice Helical CT using Dual-front Active Contours

Hua Li, Lifeng Yu, Xin Liu, Cynthia H. McCollough

Abstract— **Metallic implants may cause severe artifacts in CT exams. Suppression of metal artifacts remains to be a very challenging problem, in which metal region segmentation is one of the most important steps. We proposed a novel, semi-automatic segmentation algorithm based on the dual-front active contour model and the boundary mapping strategy to detect the metal regions on reformatted projection data, and to effectively eliminate/suppress metal artifacts on reconstructed images. Experimental studies on clinical hip and shoulder CT exams demonstrated that the proposed method was able to segment multiple metal implants more accurately relative to threshold-based methods. The artifacts caused by dense metal implants were better suppressed.**

I. Introduction

Artifacts induced by metallic implants significantly degrade the image quality and limit the diagnostic value of CT images. Iterative reconstruction methods [1, 2] are either difficult to implement in combination with the standard reconstruction algorithms in modern CT scanners or are computationally expensive for the large data sets generated by multi-slice CT scanners. Adaptive filtering has also been used with the purpose of reducing the streaking artifacts caused by photon starvation [3, 4]. Most of the metal artifact suppression methods are based on the strategy of projection modification. One procedure involves the segmentation of metal regions in reconstructed images [5-7], while the other involves the direct segmentation of metal shadows in raw projection data [8-11].

In projection modification methods, the major challenge lies in the accurate detection of metal regions either on the reconstructed images or on the raw projection data. Up to now, manual segmentation or simple thresholding methods are commonly used. Typically, one 64 multi-slice helical CT scan contains 40,000-70,000 projection views for a chest-abdomen-pelvis helical scan. It is very challenging to detect multiple metal implants on each projection frame (typically in the size of 672x32) due to the large amount of metal fragments. Yu and coauthors utilized a gradient-based thresholding method to detect the metal regions on reformatted projections, which are created from the helical projection data in multi-slice helical CT [12]. Since each reformatted projection is formed by combining data from the same view angle over the full longitudinal scan range, all of the metal objects in the scan range show up in every reformatted projection. The shape, location, number of objects, and region information of metal implants can be easily recognized from a single reformatted projection, which makes the metal detection much easier than those methods that perform metal detection on each single projection frame. In addition, there is another nice property of the reformatted projection data was not discovered yet in Yu's work. Since the rotation angle difference between adjacent reformatted projections is very small (about 0.07º), all the characteristics of metal objects only change slightly between adjacent reformatted projections. The segmented metal boundary on the previous projection is a perfect initialization that can be refined to obtain the accurate metal boundary on the current projection. Repeating this procedure may facilitate the segmentation on all the reformatted projections.

In this paper, we proposed a novel technique to suppress metal artifacts, which was based on a new boundary tracking algorithm that utilizes the dual-front active contour model and the boundary mapping strategy to extract metal regions on each reformatted projection efficiently and accurately. Then, a Delaunay triangulation is applied to fill the metal shadows. Finally, the modified projection data is load back to a scanner to reconstruct the diagnostic CT images. Experimental results on clinical cases show that the proposed algorithm can provide accurate segmentation of metal implants, and suppress metal artifacts successfully.

II. Method and Materials

A. Reformatted Projection and Pitch Correction

In multi-slice helical scan, we created the reformatted projections by combining all the frames with the same projection angle every 360º over the full longitudinal scan range. After a reformatted projection is created, the shape of the metal might not be continuous due to pitch factors. In order to provide reasonable and undistorted metal projections for the following procedure, we corrected pitch factors. When $p > 1$, we processed it as if $p = 1$. However, when $p < 1$, we ignored the data inside the overlap region on the first of every two projection frames and generated a reformatted projection without overlapping regions.

Hua Li, Ph.D, Lifeng Yu, Ph.D, Xin Liu, Ph.D, Cynthia H. McCollogh, Ph.D, are with the Department of Radiology, Mayo Clinic, Rochester, MN 55901, USA.

Email: {li.hua, yu.lifeng, liu.xin, mccollough.cynthia}@mayo.edu

B. *Metallic Object Extraction*

As discussed in Introduction, the shape, location, number of objects, and other characteristics of metal implants can be easily recognized from a single reformatted projection. Moreover, the shape and location of the metal structures only change slightly between continuous reformatted projections. Based on these observations, we proposed a novel, semi-automatic boundary tracking algorithm to extract the metal implants from 2D reformatted projection sequences. This boundary tracking algorithm consists of boundary mapping and boundary extraction. The flowchart was shown in Figure 2. First, the metal object is extracted either manually or through an automatic method on the first 2D reformatted projection. Then, the segmented boundary is mapped to the next continuous slice, and set as the initialization of the dual-front active contour models (DFAC). By utilizing the DFAC model, the boundary curve mapped from the previous slice is propagated to the actual metal object boundary in the current slice within only a couple of iterations. The boundary mapping step and the boundary tracking step are repeated until all reformatted projections are processed and the metal implant is extracted on all the projections [13].

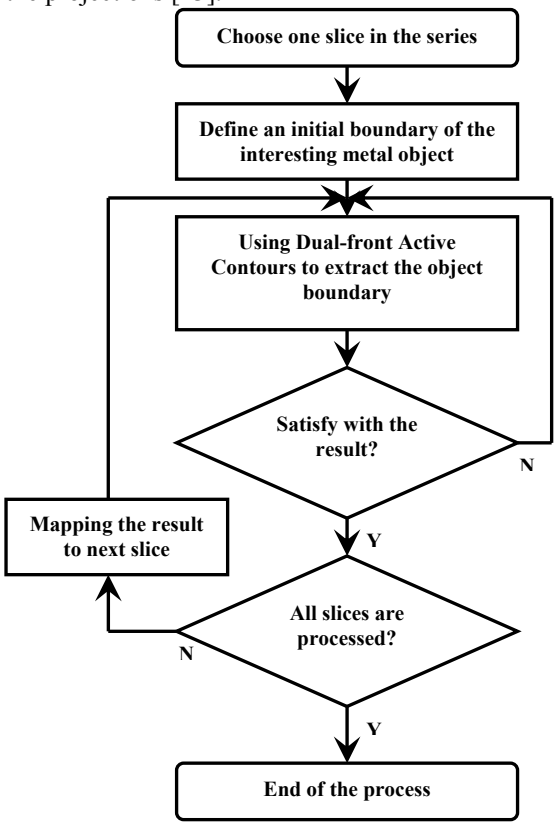

Figure 2. Flowchart depicting the steps to extract metal objects on 2D reformatted projection sequence.

Usually, metal structures only change very slightly in continuous projections. So the actual boundary obtained from the previous slice is a prefect preliminary boundary of the metal object in the current slice. Here we use a dual-front active contour model [14] to refine the preliminary boundary to the true metal implant boundary in each reformatted projection. The purpose of dual-front active contour model is to minimize an energy function in order to find "*a potential weighted global minimum partition curve*" within an active region, and then iteratively change the active region until the final objective is obtained. As shown in Figure 3, dual-front active contour model is an iterative process including the dual front evolution and active region location.

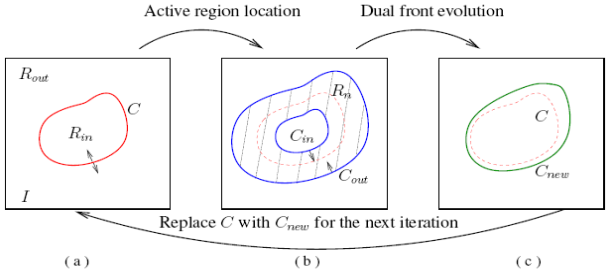

Figure 3. Iteration process of the dual-front active contour model.

For metal segmentation in this study, since the true boundary on the current slice is very close to the initialization, the mapping of the metal boundary in the previous slice, the boundary refinement can therefore be treated as a problem to find the optimal minimal partition curve which minimizes the energy functional related to the metal boundary in a narrow active region. By setting appropriate potentials based on the properties of reformatted projections, the potential weighted minimal partition curve can be equal to the metal implant boundaries. Only a couple of iterations need to propagate the initialization to the real boundary since they are very close to each other. Also, since the dual front evolution tries to find the global minimal partition curve within a specific active region instead of the whole image, the degree of this globalness may be changed easily by adjusting the size of active regions. This property enables a flexible way to extract metal implants with different sizes and shapes. Furthermore, one of the nice properties of dual-front active models is its capability to handle topology changes of the detected object during the iterative process just like standard level set evolutions. We can detect several disjoint objects with only one initial curve, which is very suitable to detect multiple metal implants such as bilateral hip prosthesis because the metal regions might be connected or separated on different projections during the whole 360º rotation.

C. *Metal shadow interpolation and image reconstruction*

After the metal object was detected and removed from each reformatted projection, a 2D interpolation was performed to fill metal shadows [15, 16]. In order to improve the computational efficiency, the interpolation was done only on a small region that includes the metal projection region plus a margin of 10 pixels. Before interpolating metal shadow regions, a median filter (size of

5×5 pixels) operator was applied to remove the isolated high value projections in the small region for smoothly interpolation. The 2D interpolation is based on a Delaunay triangulation of the data that uses Qhull [16]. The use of Qhull method is to accommodate the irregular shape of the metals possibly present in the reformatted projections. After the removal of the metal projection on the reformatted projection, the corrected raw data were written back to the original format before the pitch correction and loaded onto the scanner to perform the image reconstruction.

III. Results

We evaluated the method using clinical exams performed on 64-slice CT scanners (Sensation 64, Siemens, Germany). Figure 4 and Figure 5 showed the metal extraction and interpolation results from a contrast-enhanced abdomen CT exam. The patient had two dense metal implants in hips. The scanning parameters were as follows: 120 kVp, detector collimation 32×0.6 mm with double *z* sampling, rotation time 0.5 second, helical pitch 1.2, and quality reference mAs 240. The images were reconstructed with a slice thickness of 5 mm and a B40f kernel. As can be seen, the continuity of boundary structures in the area of interpolated projections was maintained and the artifacts were removed. Figure 6 showed the reconstructed axial, coronal, and sagittal images based on the original and corrected projection data from the same patient data in Figure 5.

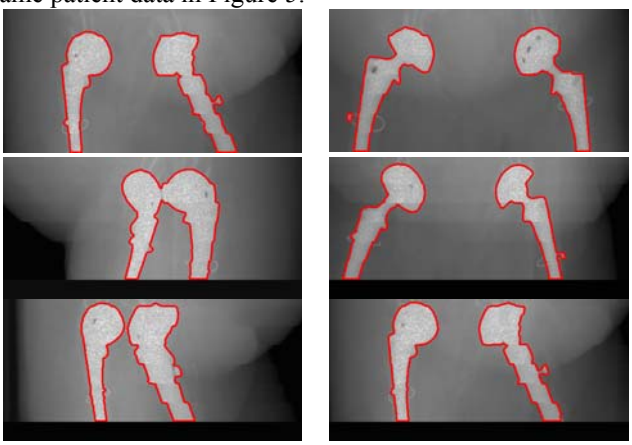

Figure 4. The metal boundary extraction on 6 different angles of the reformatted projections around the whole 360º rotation for a routine abdomen CT exam. The order of different angles is from left to right, and up to down.

Figures 7 and 8 showed the results from another patient study. This patient had a single shoulder implant. The scanning parameters were as follows: 140 kVp, detector collimation 32×0.6 mm with double z sampling, rotation time 1.0 second, helical pitch 0.45, and quality reference mAs 350. The images were reconstructed with a slice thickness of 5 mm and B40 kernel. As can be seen, streak artifacts originating from the metal were dramatically reduced with the proposed method. The shape of this shoulder metal implant is very simple while the background is complex due to the high attenuation of the shoulder. Especially when scanning along the lateral direction, the projection of two shoulders led to very bright regions that were similar to the metal region. Under this situation, it is very difficult for a threshold-based method to accurately extract the metal region. In contrast, when using the method proposed in this paper, the extraction result from the previous projection provided a good initialization for processing the current projection. The propagation principle also restricted the distortion of metal shape by setting narrow active regions. It was easy to extract metal structures from more than 4000 reformatted projections by utilizing simple parameter settings. This example illustrated the benefit of the proposed method on extracting metal structures from complex background.

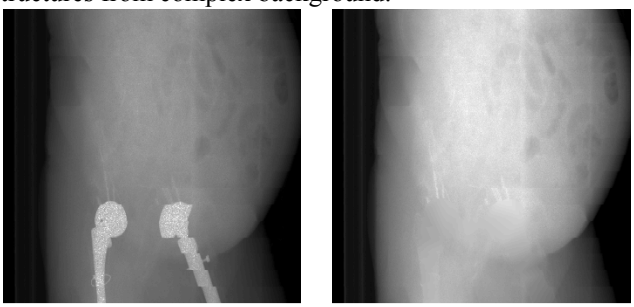

(a) (b)

Figure 5. An example of 2D metal extraction and interpolation to remove the metal projection. (a) Reformatted projection with metal regions. (b) The updated projection data with metal extraction and metal shadow interpolation.

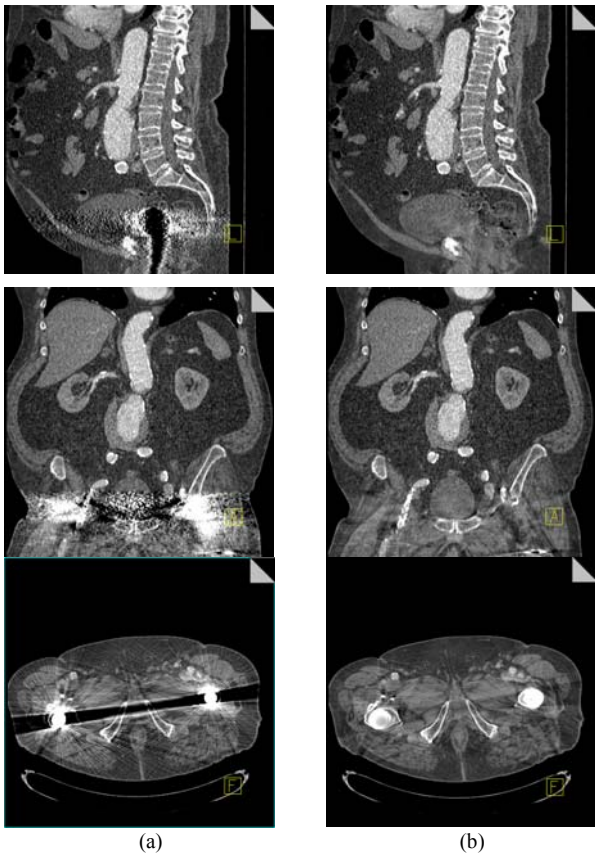

(a) (b)

Figure 6. Three example slices at sagittal, coronal, and axial planes from metal artifact reduction of the same CT exam as in Figure 5. (a) before correction, (b) after correction.

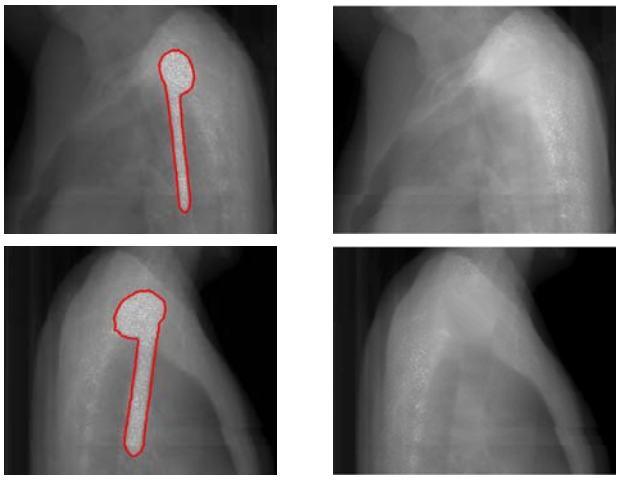

(a) (b)

Figure 7. An example of 2D metal extraction and interpolation to remove the metal projection in a shoulder CT exam. (a): Reformatted projections with labeled metal regions and the boundary extraction. (b): The updated projection data with metal removal and interpolation.

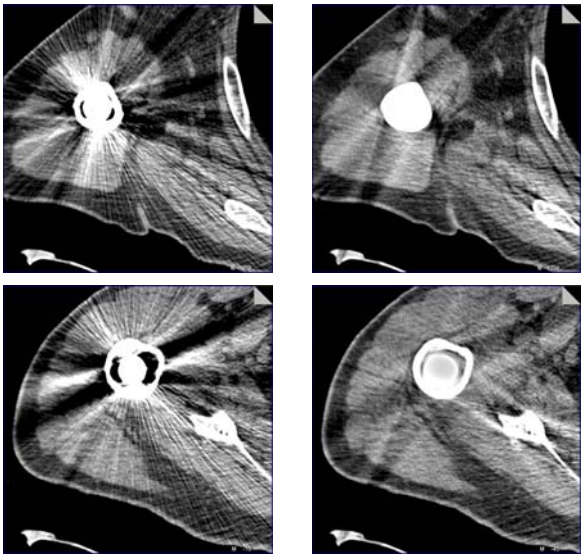

(a) (b)

Figure 8. Two axial slices from metal artifact reduction of the same CT exam in Figure 7. (a) before correction, (b) after correction.

IV. Conclusions

We proposed a novel technique to suppress metal artifacts in multi-slice helical CT by utilizing an image segmentation algorithm based on dual-front active contour models and boundary mapping strategy. The innovation of this method includes two aspects. First, the novel dual-front active contour model provides an efficient and stable strategy for metal segmentation from reformatted projections. Second, the shape, location, and other characteristics of metal structures on reformatted projects provides a good guidance for the 2D boundary mapping and segmentation strategy, which makes the metal segmentation based on the dual-front active contour model and the subsequent data correction more stable and consistent throughout the full dataset. Experimental studies on clinical hip and shoulder CT exams demonstrated that the proposed method was able to segment the metal implant more accurately relative to threshold-based methods. As a result, the artifacts caused by dense metal implants were better suppressed.

References

[1] B. De Man, J. Nuyts, P. Dupont, G. Marchal, and P. Suetens, "An iterative maximum-likelihood polychromatic algorithm for CT," *IEEE Trans Med Imaging,* vol. 20, pp. 999-1008, Oct 2001.

[2] G. Wang, D. L. Snyder, J. A. O'Sullivan, and M. W. Vannier, "Iterative deblurring for CT metal artifact reduction," *IEEE Trans Med Imaging,* vol. 15, pp. 657-64, 1996.

[3] J. Hsieh, "Adaptive streak artifact reduction in computed tomography resulting from excessive x-ray photon noise," *Med Phys,* vol. 25, pp. 2139-47, Nov 1998.

[4] M. Kachelriess, O. Watzke, and W. A. Kalender, "Generalized multi-dimensional adaptive filtering for conventional and spiral single-slice, multi-slice, and cone-beam CT," *Med Phys,* vol. 28, pp. 475-90, Apr 2001.

[5] M. Bal and L. Spies, "Metal artifact reduction in CT using tissue-class modeling and adaptive prefiltering," *Med Phys,* vol. 33, pp. 2852-9, Aug 2006.

[6] O. Watzke and W. A. Kalender, "A pragmatic approach to metal artifact reduction in CT: merging of metal artifact reduced images," *Eur Radiol,* vol. 14, pp. 849-56, May 2004.

[7] M. Yazdia, L. Gingras, and L. Beaulieu, "An adaptive approach to metal artifact reduction in helical computed tomography for radiation therapy treatment planning: Experimental and clinical studies," *International Journal of Radiation Oncology Biology Physics,* vol. 62, pp. 1224-1231, 2005.

[8] R. M. Lewitt and R. H. T. Bates, " Image reconstruction from projections: III. Projection completion methods.," *Optik* vol. 50, pp. 189-204, 1978.

[9] A. H. Mahnken, R. Raupach, J. E. Wildberger, B. Jung, N. Heussen, T. G. Flohr, R. W. Gunther, and S. Schaller, "A new algorithm for metal artifact reduction in computed tomography: in vitro and in vivo evaluation after total hip replacement," *Invest Radiol,* vol. 38, pp. 769-75, Dec 2003.

[10] S. Zhao, D. D. Robertson, G. Wang, B. Whiting, and K. T. Bae, "X-ray CT metal artifact reduction using wavelets: an application for imaging total hip prostheses," *IEEE Trans Med Imaging,* vol. 19, pp. 1238-47, Dec 2000.

[11] Y. Zhang, L. Zhang, X. R. Zhu, A. K. Lee, M. Chambers, and L. Dong, "Reducing metal artifacts in cone-beam CT images by preprocessing projection data," *Int J Radiat Oncol Biol Phys,* vol. 67, pp. 924-32, Mar 1 2007.

[12] L. Yu, J. M. Kofler, X. Liu, A. N. Primak, and C. H. McCollough, "WE-D-332-07: Automatic Metal Artifact Reduction From Reformatted Projections in Multi-Slice Helical CT," *Med Phys* vol. 35, pp. 2949-49, June 2008.

[13] H. Li, A. Elmoataz, J. Fadili, S. Ruan, and B. Romaniuk, "3D medical image segmentation approach based on multi-label front propagation," in *Image Processing, 2004. ICIP '04. 2004 International Conference on*, 2004, pp. 2925-2928 Vol. 5.

[14] H. Li and A. Yezzi, "Local or global minima: flexible dual-front active contours," *IEEE Trans Pattern Anal Mach Intell,* vol. 29, pp. 1-14, Jan 2007.

[15] L. Yu, et al., "Metal Artifact Reduction from Reformatted Projections in Multi-slice Helical CT: Techniques and Initial Clinical Results," *Medical Physics,* 2008.

[16] C. B. Barber, D. P. Dobkin, and H. Huhdanpaa, "The Quickhull Algorithm for Convex Hulls," *ACM Transactions on Mathematical Software,* vol. 22, pp. 469-483, 1996.